

Quantum quenches and many-body localization in the thermodynamic limit

Baoming Tang,^{1,2} Deepak Iyer,¹ and Marcos Rigol¹

¹*Department of Physics, The Pennsylvania State University, University Park, PA 16802, USA*

²*Department of Physics, Georgetown University, Washington, DC 20057, USA*

We use thermalization indicators and numerical linked cluster expansions to probe the onset of many-body localization in a disordered one-dimensional hard-core boson model in the thermodynamic limit. We show that after equilibration following a quench from a delocalized state, the momentum distribution indicates a freezing of one-particle correlations at higher values than in thermal equilibrium. The position of the delocalization to localization transition, identified by the breakdown of thermalization with increasing disorder strength, is found to be consistent with the value from the level statistics obtained via full exact diagonalization of finite chains. Our results strongly support the existence of a many-body localized phase in the thermodynamic limit.

PACS numbers: 05.30.Jp, 75.10.Pq, 71.30.+h, 05.50.+q

Since the first quantitative discussion of localization by Anderson in 1958 [1], a large number of experiments have revealed phenomena governed by localization physics in solid state [2, 3] and atomic [4–7] physics. In the absence of interactions, destructive interference due to scattering off of impurities is responsible for localization [1]. What happens in the presence of interactions has remained an open problem whose exploration has become an active area of research over the past few years. For weak interactions, perturbative arguments support the existence of localized phases [8–11]. For strong interactions, on the other hand, numerical studies have found signatures of many-body localization and have explored its implications [12–24]. Nonetheless, it remains a challenge to conclusively establish that, in the presence of strong interactions, the delocalization to localization transition occurs at finite disorder strength in the thermodynamic limit.

The signatures of localization in experiments are mostly dynamical in nature, e.g., measurements of the conductivity [3]. Theoretically, it is difficult to study dynamical quantities. So, to identify many-body localized phases, it is common to use the statistics of the energy level spacing instead (see, e.g., Refs. [12, 14, 15]). Poissonian level statistics is expected for localized phases, whereas Wigner-Dyson statistics is expected for delocalized ones. Equally accessible to experimental and theoretical studies is a defining, but less explored, signature of many-body localization—when taken far from equilibrium, isolated localized systems do not thermalize [25].

Relaxation dynamics and thermalization in isolated many-body quantum systems is a very active area of current research on its own [26–28]. There is growing evidence that generic many-body quantum systems thermalize after being taken far from equilibrium [29–34], and that this is a consequence of eigenstate thermalization [29–31, 35–46]. That is, thermalization results from the fact that, for few-body observables, individual eigenstates of the Hamiltonian already exhibit thermal properties [29, 35, 36]. This can be pictured as the system effectively acting as its own bath. Such a picture breaks down in integrable systems [29–31] and in many-body localized ones. In the latter, different parts of the system

cannot communicate with one another, i.e., they cannot be ergodic [25]. Numerical calculations in finite systems have provided evidence of the breakdown of eigenstate thermalization [15] and thermalization [15, 47] in disordered many-body systems.

Here, we study quantum quenches in disordered isolated systems in the thermodynamic limit. By a quantum quench it is meant that the initial state is stationary with respect to an initial Hamiltonian, which is suddenly changed to a new (time-independent) Hamiltonian. The latter then drives the (unitary) dynamics of the system. We are interested in the time average of observables (say, \hat{O}) after the quench. They can be calculated as $\overline{O(\tau)} = \text{Tr}[\hat{\rho}(\tau)\hat{O}] = \text{Tr}[\hat{\rho}(\tau)\hat{O}] \equiv \text{Tr}[\hat{\rho}_{\text{DE}}\hat{O}] = O_{\text{DE}}$, where $\overline{(\cdot)} = \lim_{\tau' \rightarrow \infty} 1/\tau' \int_0^{\tau'} d\tau (\cdot)$ indicates the infinite time average, $\hat{\rho}(\tau)$ is the density matrix of the time-evolving state, and $\hat{\rho}_{\text{DE}} \equiv \hat{\rho}(\tau)$ is the density matrix of the so-called diagonal ensemble (DE) [29]. To obtain results in the thermodynamic limit, we advance a recently introduced numerical linked cluster expansion (NLCE) for the DE [34, 48, 49]. NLCEs for systems in thermal equilibrium were introduced in Refs. [50, 51], and their implementation was discussed in Ref. [52]. When converged, NLCE calculations provide exact results in the thermodynamic limit. For quenches in the integrable XXZ chain, this was shown in Refs. [44, 45] by comparing NLCEs with exact analytic calculations using the Bethe ansatz. In this Rapid Communication, thermalization, or the lack thereof, is studied by comparing results for observables in the DE and in the grand-canonical ensemble (GE).

We focus on a system of impenetrable bosons in one-dimension (1D) with Hamiltonian $\hat{H} = \hat{H}_0 + \hat{H}_D$, where

$$\hat{H}_0 = \sum_i \left[-t(\hat{b}_i^\dagger \hat{b}_{i+1} + \text{H.c.}) + V \left(\hat{n}_i - \frac{1}{2} \right) \left(\hat{n}_{i+1} - \frac{1}{2} \right) \right] \quad (1)$$

is translationally invariant and $\hat{H}_D = \sum_i h_i (\hat{n}_i - \frac{1}{2})$ is the term with the disorder. \hat{b}_i^\dagger (\hat{b}_i) creates (annihilates) a hard-core boson at site i and $\hat{n}_i = \hat{b}_i^\dagger \hat{b}_i$ is the site number operator. t stands for the hopping parameter, V for

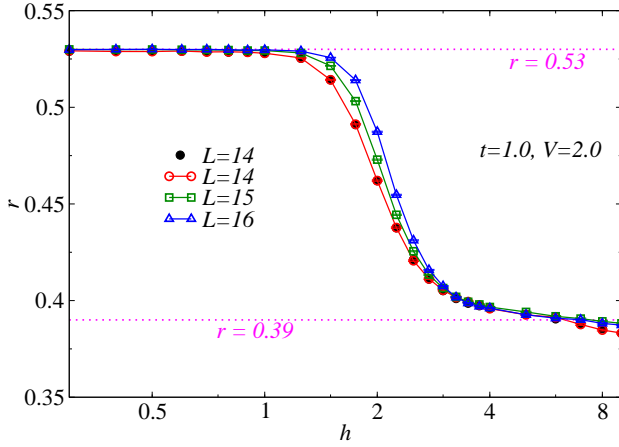


FIG. 1. (Color online) Exact diagonalization results for the averaged ratio of two consecutive energy gaps r (see text) as a function of disorder strength in chains with $L = 14, 15$, and 16 sites, and $V = 2$. For $L = 14$, the energy ratio was computed considering all $2^{14} = 16384$ disorder field configurations (solid circles). We also show the energy ratio for $L = 14$ (open circles), $L = 15$ (open squares), and $L = 16$ (open triangles) averaging over 9100 random samples. The error bars depict one standard deviation. They make apparent that the statistical errors are negligible at the scale of the figure.

the nearest neighbor interaction, and h_i for the strength of the on-site disorder. In the spin language, \hat{H} describes a spin-1/2 XXZ model in the presence of a random magnetic field in the z direction. We select the random field to have a binary distribution with equal probabilities for $h_i = \pm h$. This model has been recently motivated in the context of ultracold bosons in optical lattices [21].

We first use full exact diagonalization of finite chains with open boundary conditions to check whether \hat{H} supports a many-body localized phase (as argued in Ref. [21]) and, if it does, the value of the disorder strength at which such a phase appears. We focus on $V = 2t$ (which is the Heisenberg point in the spin model) and set $t = 1$ as our unit of energy. As a first indicator of many-body localization, we study the averaged ratio of the smaller and the larger of two consecutive energy gaps, $r_n = \min[\delta_{n-1}^E, \delta_n^E] / \max[\delta_{n-1}^E, \delta_n^E]$, where $\delta_n^E \equiv E_{n+1} - E_n$ is the difference between adjacent energy levels in the spectrum [12, 14]. The averaged ratio r is obtained by averaging r_n over the central half of the spectrum for a given disorder configuration, and then averaging over disorder configurations. In the delocalized phase, one expects $r \approx 0.5359$ and in the localized one, $r \approx 0.3863$, corresponding to the results for the Wigner-Dyson and Poissonian distributions [53], respectively.

Figure 1 shows the averaged ratio r as a function of the strength of the random field h for three system sizes. One can see that there is a transition from a delocalized to a localized phase with increasing disorder strength, and that it sharpens with increasing system size. From the delocalized side, with increasing h , the curves for

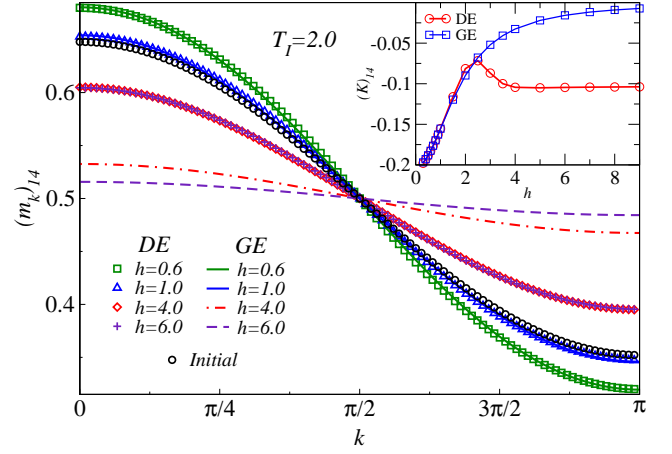


FIG. 2. (Color online) Last order ($l = 14$) of the NLCE calculation for the momentum distribution in the initial state with $T_I = 2$, and in the DE and GE after quenches with four different values of the disorder strength h (two below and two above the delocalization to localization transition). The inset depicts the last order of the NLCE for the kinetic energy K after quenches as a function of h . Note that, for $h \lesssim 2.5 < h_c$, the results in the DE and the GE are virtually indistinguishable.

different system sizes meet in the vicinity of $h = 3.5$, suggesting that the critical $h_c \approx 3.5$. Remarkably, for the same model but with continuous disorder, the transition was found to be at around twice this value ($h_c \approx 7$) [14].

Now that we have an idea of the disorder strengths that correspond to the ergodic and many-body localized phases, we proceed to study quantum quenches into both regimes. We take the initial state to be in thermal equilibrium at some temperature T_I for \hat{H}_I with parameters $t_I = 0.5$, $V_I = 2.5$, and $h_j = 0$ for all j , i.e., the initial state is homogeneous. (We have verified that the results reported are robust when changing the initial state, which is, in principle, arbitrary.) After the quench, we take $t = 1$, $V = 2.0$, and different values of $h \neq 0$ (as in Fig. 1). In all our calculations, the chemical potential $\mu = 0$, so that the systems are at half filling. NLCEs for the diagonal ensemble allow one to compute the infinite-time average of observables in the thermodynamic limit for lattice systems evolving unitarily [34, 49]. The fundamental NLCE development introduced in this Rapid Communication is the ability to deal with systems with disorder.

In translationally invariant systems, NLCEs allow one to calculate the expectation value of an extensive observable per lattice site in the thermodynamic limit, \mathcal{O} , as a sum over the contributions from all clusters c that can be embedded on the infinite lattice: $\mathcal{O} = \sum_c M(c) \times W_{\mathcal{O}}(c)$, where $M(c)$ is the multiplicity of c , defined as the number of ways per site in which cluster c can be embedded on the lattice. $W_{\mathcal{O}}(c)$ is the weight of \mathcal{O} in cluster c , which is calculated recursively using the inclusion-exclusion principle $W_{\mathcal{O}}(c) = \mathcal{O}(c) - \sum_{s \subset c} W_{\mathcal{O}}(s)$, where $\mathcal{O}(c) = \text{Tr}[\hat{\mathcal{O}} \hat{\rho}_c]$ is computed using full exact diagonalization, with $\hat{\rho}_c$ be-

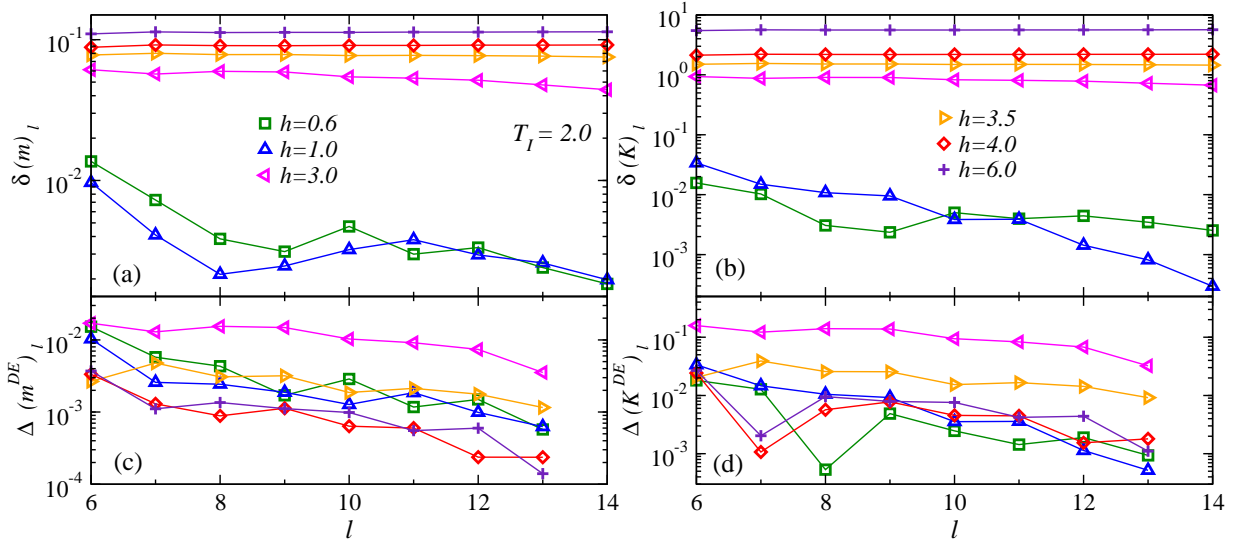


FIG. 3. (Color online) Relative differences for the momentum distribution and the kinetic energy vs l in the NLCE calculation for six values of h and $T_I = 2$. (a) $\delta(m)_l$, (b) $\delta(K)_l$, (c) $\Delta(m^{\text{DE}})_l$, and (d) $\Delta(K^{\text{DE}})_l$. Results for $\Delta(m^{\text{GE}})_l$ and $\Delta(K^{\text{GE}})_l$ are reported in Ref. [54]. For $h = 4$ and 5 , the results for $\delta(m)_l$ and $\delta(K)_l$ do not change with changing l , i.e., they have converged.

ing the density matrix relevant to the calculation [e.g., of the grand-canonical ensemble (GE) or the diagonal ensemble (DE)] in cluster c [34, 49].

Such an expansion cannot be applied to systems in which translational symmetry is broken, e.g., by disorder. However, a disorder average that restores an exact translational invariance enables once again the use of NLCEs. The two crucial points that make that possible are: (i) the linear character of the equations defining the linked cluster expansion, so that disorder average can be commuted with the NLCE summation process, and (ii) the use of binary disorder which, after averaging over all possible disorder realizations, restores the translational symmetry (and also particle-hole symmetry) of \hat{H}_0 . Hence, all we need to do in our calculations is replace $\mathcal{O}(c) = \text{Tr}[\hat{\mathcal{O}}\hat{\rho}_c]$ for the translationally invariant case by:

$$\mathcal{O}(c) = \left\langle \text{Tr}[\hat{\mathcal{O}}\hat{\rho}_c] \right\rangle_{\text{dis}}, \quad (2)$$

where $\langle \cdot \rangle_{\text{dis}}$ represents the disorder average. Having to compute this additional average reduces our site based linked cluster expansion from a maximum of 18 sites for translationally invariant systems [34, 48, 49] to 14 sites here. We define $\mathcal{O}_l^{\text{ens}}$ as the sum over the contributions of clusters with up to l sites, where “ens” could be DE or GE. The temperature used in the GE calculations to describe the system after the quench is determined from a comparison of the energy of DE and the GE by ensuring that $|E_{14}^{\text{DE}} - E_{14}^{\text{GE}}|/|E_{14}^{\text{DE}}| < 10^{-12}$. We only report results for values of T_I for which E_{14}^{DE} and E_{14}^{GE} are converged within machine precision (see Ref. [54]).

In Fig. 2, we report the initial momentum distribution of a system with $T_I = 2$ and the final momentum distribution for different values of h after the quench. After the quench, the DE and GE results for $h = 0.6$

and 1 ($h < h_c$) are indistinguishable from each other, while for $h = 4$ and 6 ($h > h_c$) they are very different from each other. Remarkably, the results that are close to each other for $h > h_c$ are those from the DE. The contrast between the DE and GE results in this regime makes apparent that there is more coherence in the one-particle sector after equilibration than if the system were in thermal equilibrium ($m_{k=0}^{\text{DE}} > m_{k=0}^{\text{GE}}$). The system “remembers” one-particle correlations from the initial state. This has also been seen in quasiperiodic systems [55]. It is easy to understand in the limit of very strong disorder, where $\hat{H} = \sum_i h_i(\hat{n}_i - \frac{1}{2})$, and, in the Heisenberg picture, $\hat{b}_i^\dagger(\tau)\hat{b}_j(\tau) = \exp[i(h_i - h_j)\tau/\hbar]\hat{b}_i^\dagger(0)\hat{b}_j(0)$. A disorder average over h_i, h_j (with each being $\pm h$ with equal likelihood) reveals that, for a half-filled system, $m_k^{\text{DE}} = 1/4 + m_k(\tau = 0)/2$. Strikingly, a very strong freezing of correlations is seen right after entering the many-body localized phase. The results for the kinetic energy, almost constant in the inset in Fig. 2 for $h > h_c$, provide evidence of the robustness of these findings.

To discern which of the differences between the DE and GE seen in Fig. 2 are due to lack of convergence of the NLCE and which are expected to survive in the thermodynamic limit, we calculate the following two differences,

$$\delta(m)_l = \frac{\sum_k |(m_k)_l^{\text{DE}} - (m_k)_l^{\text{GE}}|}{\sum_k |(m_k)_l^{\text{GE}}|}, \quad (3)$$

which allows us to quantify the difference between the DE and the GE, and

$$\Delta(m^{\text{ens}})_l = \frac{\sum_k |(m_k)_l^{\text{ens}} - (m_k)_{14}^{\text{ens}}|}{\sum_k |(m_k)_{14}^{\text{ens}}|}, \quad (4)$$

which allows us to estimate the convergence of the NLCE calculations [34]. $\delta(K)_l$ and $\Delta(K^{\text{ens}})_l$ follow straightforwardly from Eqs. (3) and (4), respectively, by removing

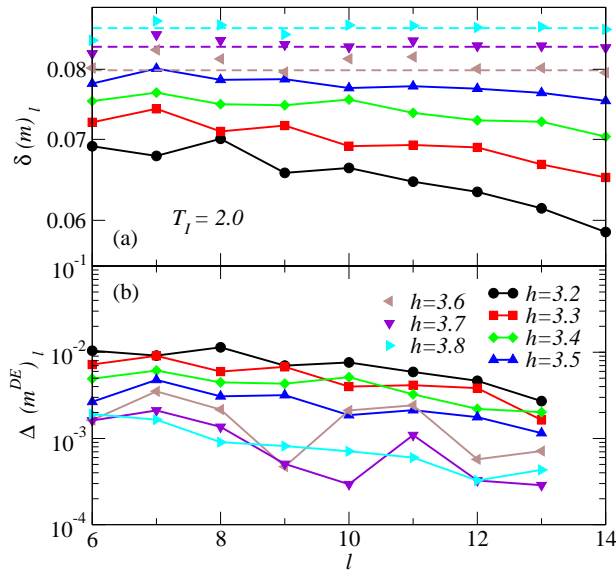


FIG. 4. (Color online) Relative differences for the momentum distribution vs l in the NLCE calculation for $3.2 \leq h \leq 3.8$. (a) $\delta(m)_l$ and (b) $\Delta(m^{\text{DE}})_l$. In (a), horizontal dashed lines correspond to the average value of last two orders of $\delta(m)_l$ for $h = 3.6, 3.7$, and 3.8 .

the sums and replacing $m_k \rightarrow K$. For the GE calculations when $T_I > 1$, $(m_k)_{14}^{\text{GE}}$ and K_{14}^{GE} are converged within machine precision (see Ref. [54]).

Results for $\delta(m)_l$, $\delta(K)_l$, $\Delta(m^{\text{DE}})_l$, and $\Delta(K^{\text{DE}})_l$ vs l are reported in Figs. 3(a)–3(d), respectively, for six values of h . They show the following: (i) The momentum distribution function (a nonlocal quantity) and the kinetic energy (a local quantity) exhibit qualitatively similar behavior. (ii) For $h \gtrsim 3.5$, $\delta(m)_l$ and $\delta(K)_l$ do not change with increasing l , and are much larger than $\Delta(m^{\text{DE}})_l$ and $\Delta(K^{\text{DE}})_l$, i.e., the former are expected to remain nonzero in the thermodynamic limit. This supports the existence of many-body localization in the thermodynamic limit. (iii) For $h \lesssim 3.0$, $\delta(m)_l$ and $\delta(K)_l$ decrease with increasing l , and are of the same order of magnitude as $\Delta(m^{\text{DE}})_l$ and $\Delta(K^{\text{DE}})_l$ (which also decrease with increasing system size). Hence, the differences between those observables in the DE and the GE are expected to vanish in the thermodynamic limit, i.e., those values of h belong to the ergodic phase. In this phase, $\delta(m)_l$ and $\delta(K)_l$ behave as in systems without disorder [34]. (iv) $\Delta(m^{\text{DE}})_l$

and $\Delta(K^{\text{DE}})_l$ in Figs. 3(c) and 3(d) show that the NLCE convergence errors are largest in the region where the system transitions between ergodic and localized.

In order to better pin down the transition point between the ergodic and many-body localized phases, in Fig. 4(a) we plot $\delta(m)_l$ vs l in the vicinity of $h = 3.5$. For $h \geq 3.6$, we see that $\delta(m)_l$ seems to saturate to a finite value that is larger than $\Delta(m^{\text{DE}})_{13}$, suggesting that the system is many-body localized for $h \geq 3.6$. The transition between ergodic and many-body localized can occur for smaller values of h as, for larger values of l , the plots for $\delta(m)_l$ may saturate to a constant value. However, we expect that $h_c \approx 3.5$ since in the vicinity of this disorder strength we see that $\delta(m)_l$ and $\Delta(m^{\text{DE}})_{l-1}$ are very close to each other for the largest system sizes studied. We should stress that, for $T_I > 2$, we do not find indications that h_c increases significantly with increasing T_I [54]. In general, it is expected that, as one increases the mean energy density after the quench (which is exactly what increasing T_I does in our case), the transition point between the delocalized and localized phases should move towards stronger disorder [19]. In the systems studied here, it is likely that a $T_I < 2$ is needed to clearly observe that effect. However, the failure of NLCE to converge in that regime does not allow us to check it.

In summary, we have studied quantum quenches in the thermodynamic limit in an interacting model with binary disorder. This was possible by generalizing the NLCE approach introduced in Ref. [34] to solve problems with disorder. We have shown that for quenches starting in a delocalized phase, a freezing of correlations can occur in the steady state after the quench right after entering the many-body localized phase. We located the critical value of the transition between the ergodic and many-body localized phase using a quantum chaos indicator (the average ratio between consecutive energy gaps) in finite systems and the difference between NLCE predictions for observables in the DE and the GE after quantum quenches. The values of h_c were found to be consistent in those two schemes. The small convergence errors of NLCE for $h > h_c$ strongly support that the many-body localized phase occurs in the thermodynamic limit. We should stress that the NLCE approach introduced here can be used to study disordered systems in equilibrium [56] and after quenches [57] in two (or higher) dimensions.

Acknowledgments. This work was supported by the Office of Naval Research.

[1] P. W. Anderson, Phys. Rev. **109**, 1492 (1958).
[2] P. A. Lee and T. V. Ramakrishnan, Rev. Mod. Phys. **57**, 287 (1985).
[3] B. Kramer and A. MacKinnon, Rep. Prog. Phys. **56**, 1469 (1993).
[4] J. E. Bayfield and D. W. Sokol, Phys. Rev. Lett. **61**, 2007 (1988).

[5] J. E. Bayfield, G. Casati, I. Guarneri, and D. W. Sokol, Phys. Rev. Lett. **63**, 364 (1989).
[6] C. F. Bharucha, J. C. Robinson, F. L. Moore, B. Sundaram, Q. Niu, and M. G. Raizen, Phys. Rev. E **60**, 3881 (1999).
[7] G. Roati, C. D'Errico, L. Fallani, M. Fattori, C. Fort, M. Zaccanti, G. Modugno, M. Modugno, and M. Inguscio, Nature **453**, 895 (2008).

- [8] L. Fleishman and P. W. Anderson, Phys. Rev. B **21**, 2366 (1980).
- [9] B. L. Altshuler, Y. Gefen, A. Kamenev, and L. S. Levitov, Phys. Rev. Lett. **78**, 2803 (1997).
- [10] I. V. Gornyi, A. D. Mirlin, and D. G. Polyakov, Phys. Rev. Lett. **95**, 206603 (2005).
- [11] D. Basko, I. Aleiner, and B. Altshuler, Ann. Phys. **321**, 1126 (2006).
- [12] V. Oganesyan and D. A. Huse, Phys. Rev. B **75**, 155111 (2007).
- [13] M. Žnidarič, T. Prosen, and P. Prelovšek, Phys. Rev. B **77**, 064426 (2008).
- [14] A. Pal and D. A. Huse, Phys. Rev. B **82**, 174411 (2010).
- [15] E. Khatami, M. Rigol, A. Relaño, and A. M. Garcia-Garcia, Phys. Rev. E **85**, 050102(R) (2012).
- [16] J. H. Bardarson, F. Pollmann, and J. E. Moore, Phys. Rev. Lett. **109**, 017202 (2012).
- [17] R. Vosk and E. Altman, Phys. Rev. Lett. **110**, 067204 (2013).
- [18] M. Serbyn, Z. Papić, and D. A. Abanin, Phys. Rev. Lett. **110**, 260601 (2013).
- [19] J. A. Kjäll, J. H. Bardarson, and F. Pollmann, Phys. Rev. Lett. **113**, 107204 (2014).
- [20] T. Grover, arXiv:1405.1471.
- [21] F. Andraschko, T. Enss, and J. Sirker, Phys. Rev. Lett. **113**, 217201 (2014).
- [22] R. Vasseur, S. A. Parameswaran, and J. E. Moore, arXiv:1407.4476.
- [23] E. Altman and R. Vosk, arXiv:1408.2834.
- [24] M. Serbyn, Z. Papić, and D. A. Abanin, Phys. Rev. B **90**, 174302 (2014).
- [25] R. Nandkishore and D. A. Huse, Annu. Rev. Condens. Matt. Phys. **6**, 15 (2015).
- [26] M. A. Cazalilla and M. Rigol, New J. Phys. **12**, 055006 (2010).
- [27] J. Dziarmaga, Adv. Phys. **59**, 1063 (2010).
- [28] A. Polkovnikov, K. Sengupta, A. Silva, and M. Vengalattore, Rev. Mod. Phys. **83**, 863 (2011).
- [29] M. Rigol, V. Dunjko, and M. Olshanii, Nature **452**, 854 (2008).
- [30] M. Rigol, Phys. Rev. Lett. **103**, 100403 (2009).
- [31] M. Rigol, Phys. Rev. A **80**, 053607 (2009).
- [32] M. Eckstein, M. Kollar, and P. Werner, Phys. Rev. Lett. **103**, 056403 (2009).
- [33] M. C. Bañuls, J. I. Cirac, and M. B. Hastings, Phys. Rev. Lett. **106**, 050405 (2011).
- [34] M. Rigol, Phys. Rev. Lett. **112**, 170601 (2014).
- [35] J. M. Deutsch, Phys. Rev. A **43**, 2046 (1991).
- [36] M. Srednicki, Phys. Rev. E **50**, 888 (1994).
- [37] L. F. Santos and M. Rigol, Phys. Rev. E **82**, 031130 (2010).
- [38] G. Roux, Phys. Rev. A **81**, 053604 (2010).
- [39] M. Rigol and M. Srednicki, Phys. Rev. Lett. **108**, 110601 (2012).
- [40] C. Neuenhahn and F. Marquardt, Phys. Rev. E **85**, 060101 (2012).
- [41] E. Khatami, G. Pupillo, M. Srednicki, and M. Rigol, Phys. Rev. Lett. **111**, 050403 (2013).
- [42] R. Steinigeweg, J. Herbrych, and P. Prelovšek, Phys. Rev. E **87**, 012118 (2013).
- [43] W. Beugeling, R. Moessner, and M. Haque, Phys. Rev. E **89**, 042112 (2014).
- [44] S. Sorg, L. Vidmar, L. Pollet, and F. Heidrich-Meisner, Phys. Rev. A **90**, 033606 (2014).
- [45] W. Beugeling, R. Moessner, and M. Haque, Phys. Rev. B **91**, 012144 (2015).
- [46] H. Kim, T. N. Ikeda, and D. A. Huse, Phys. Rev. E **90**, 052105 (2014).
- [47] C. Gogolin, M. P. Müller, and J. Eisert, Phys. Rev. Lett. **106**, 040401 (2011).
- [48] B. Wouters, J. De Nardis, M. Brockmann, D. Fioretto, M. Rigol, and J.-S. Caux, Phys. Rev. Lett. **113**, 117202 (2014).
- [49] M. Rigol, Phys. Rev. E **90**, 031301(R) (2014).
- [50] M. Rigol, T. Bryant, and R. R. P. Singh, Phys. Rev. Lett. **97**, 187202 (2006).
- [51] M. Rigol, T. Bryant, and R. R. P. Singh, Phys. Rev. E **75**, 061118 (2007).
- [52] B. Tang, E. Khatami, and M. Rigol, Comput. Phys. Commun. **184**, 557 (2013).
- [53] Y. Y. Atas, E. Bogomolny, O. Giraud, and G. Roux, Phys. Rev. Lett. **110**, 084101 (2013).
- [54] See Supplemental Material for details regarding the convergence of NLCEs as a function of temperature.
- [55] C. Gramsch and M. Rigol, Phys. Rev. A **86**, 053615 (2012).
- [56] B. Tang, D. Iyer, M. Rigol, arXiv:1501.00990.
- [57] B. Tang, D. Iyer, M. Rigol (unpublished).

Supplemental Material

Convergence of NLCEs for the DE and the GE

NLCEs, when converged, give exact results in the thermodynamic limit. Here, we check the convergence of the calculations. We define the difference

$$\Delta(\mathcal{O}^{\text{ens}})_l \equiv \frac{|\mathcal{O}_l^{\text{ens}} - \mathcal{O}_{14}^{\text{ens}}|}{|\mathcal{O}_{14}^{\text{ens}}|}, \quad (5)$$

where \mathcal{O} is either the kinetic energy K or the energy E . For the momentum, we define

$$\Delta(m^{\text{ens}})_l = \frac{\sum_k |(m_k)_l^{\text{ens}} - (m_k)_{14}^{\text{ens}}|}{\sum_k |(m_k)_{14}^{\text{ens}}|}, \quad (6)$$

where m_k is the momentum distribution function. In all cases, “ens” refers to either the diagonal ensemble (DE) or the grand-canonical ensemble (GE).

In order to determine the initial temperature T_I for which the various observables calculated using NLCEs in the DE and GE are well converged, we plot $\Delta(E^{\text{ens}})_{13}$ in Fig. 5(a), $\Delta(K^{\text{ens}})_{13}$ in Fig. 5(b), and $\Delta(m^{\text{ens}})_{13}$ in Fig. 5(c) as a function of T_I for the same set of quenches as in Fig. 3 in the main text. Figure 5 shows that, with increasing T_I , $\Delta(E^{\text{GE}})_{13}$, $\Delta(K^{\text{GE}})_{13}$, $\Delta(m^{\text{GE}})_{13}$ decrease and become zero within machine precision for $T_I > 1.0$.

We therefore expect that, within the cluster sizes accessible to us, E , K , and m in the GE have converged to the thermodynamic limit results for $T_I > 1.0$. In the DE, however, only the energy [Fig. 5(a)] converges within machine precision. As evident from Figs. 5(b) and 5(c), for the kinetic energy and the momentum distributions, respectively, the relative errors do not change much with increasing temperature for $T_I > 1.0$. For these observ-

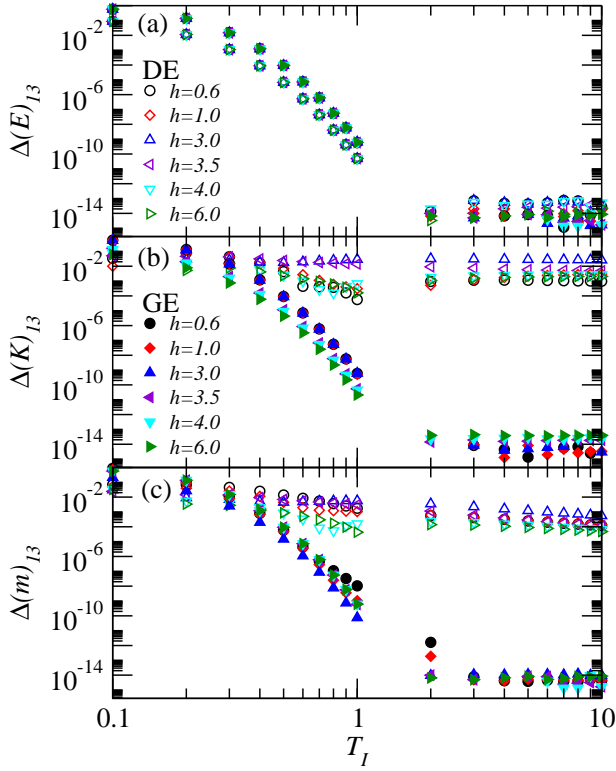


FIG. 5. (Color online) Results for: (a) $\Delta(E^{\text{ens}})_{13}$, (b) $\Delta(K^{\text{ens}})_{13}$, and (c) $\Delta(m^{\text{ens}})_{13}$ as a function of T_I for the same set of quenches as in Fig. 3 in the main text. Open (filled) symbols depict the relative differences in the DE (GE). In all panels, the GE results appear converged within machine precision for temperatures $T_I \gtrsim 2$. For the DE, only the energy (a) converges within machine precision.

ables in the DE, the error can only be reduced by considering larger system sizes.

Critical disorder strength at higher temperature

In Fig. 6, we show the equivalent of Fig. 4 but for higher initial temperatures. As mentioned there, a higher temperature is expected to increase the value of the critical strength required for the localized phase to appear. However, for the temperatures at which our NLCEs for the energy converge within machine precision, we do not observe any significant difference between the results for $T_I = 2, 10$, and 100 . This is possibly because $T_I = 2$ is already too high to see this effect. The effective temperatures after the quench are reported in Table I.

TABLE I. Effective temperatures used in the GE calculations

T_I	$h = 0.6$	$h = 1.0$	$h = 3.0$	$h = 3.5$	$h = 4.0$	$h = 6.0$
2.0	2.996	3.482	9.900	12.558	15.635	32.095
10.0	14.894	17.590	51.858	65.850	82.005	168.226
100.0	149.283	177.563	531.698	675.640	841.738	1727.657

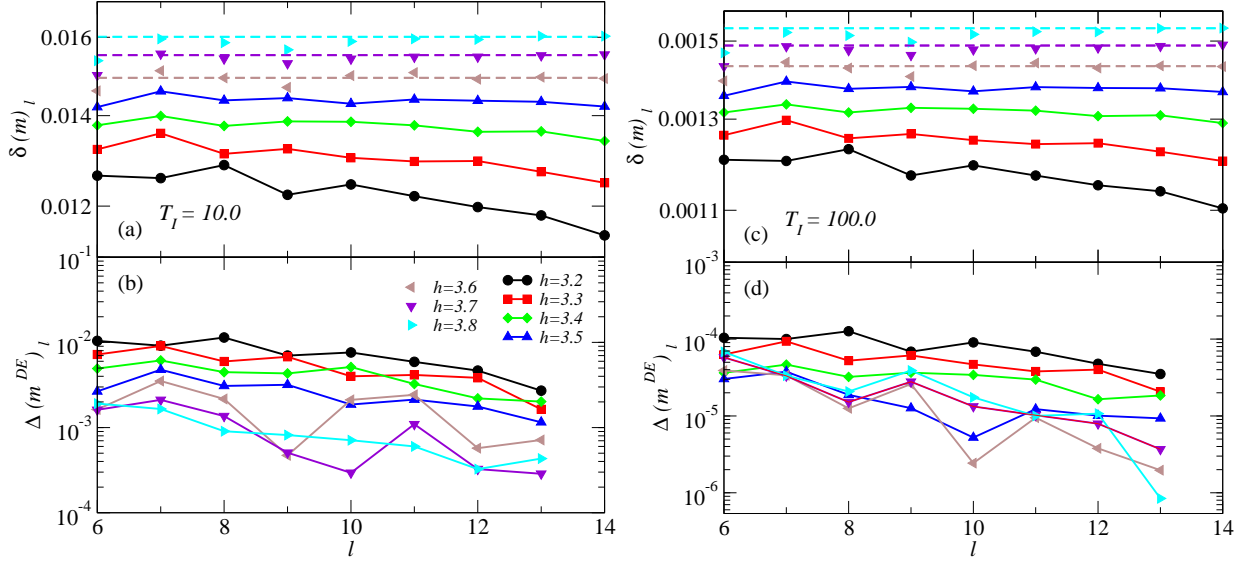


FIG. 6. (Color online) The equivalent of Fig. 4 in the main text for $T_I = 10$ (left) and $T_I = 100$ (right). For $h \geq 3.6$, $\delta(m)_l$ vs l [(a) and (c)] appears to converge to a nonzero value with increasing system size. Furthermore, the convergence errors [estimated by $\Delta(m^{\text{DE}})_l$, see panels (b) and (d)] are smaller than the $\delta(m)_l$ differences for those values of h . These results are very similar to those for $T_I = 2$ reported in the main text.